Fractionation of the Methane Isotopologues $^{13}CH_4$, $^{12}CH_3D$, and $^{13}CH_3D$ During Aerobic Oxidation of Methane by Methylococcus Capsulatus (Bath)

Citation: Wang, David T. et al. "Fractionation of the Methane Isotopologues $^{13}CH_4$, $^{12}CH_3D$, and $^{13}CH_3D$ During Aerobic Oxidation of Methane by Methylococcus Capsulatus (Bath)." Geochimica et Cosmochimica Acta 192 (November 2016): 186–202 © 2016 Elsevier

As Published: https://doi.org/10.1016/j.gca.2016.07.031

Publisher: Elsevier

Persistent URL: http://hdl.handle.net/1721.1/118880

Version: Author's final manuscript: final author's manuscript post peer review, without publisher's formatting or copy editing

Title:

Fractionation of the methane isotopologues $^{13}CH_4$, $^{12}CH_3D$, and $^{13}CH_3D$ during aerobic oxidation of methane by *Methylococcus capsulatus* (Bath) [140 char w/ spaces]

A manuscript revised for *Geochimica et Cosmochimica Acta* on 24 August 2017

Authors and affiliations:

David T. Wang[a,b,*], Paula V. Welander[c], and Shuhei Ono[a]

[a]Department of Earth, Atmospheric and Planetary Sciences, Massachusetts Institute of Technology, Cambridge, Massachusetts 02139, USA.
[b]Marine Chemistry and Geochemistry Department, Woods Hole Oceanographic Institution, Woods Hole, Massachusetts 02543, USA.
[c]Earth System Science Department, Stanford University, Stanford, California 94305, USA.

* To whom correspondence should be addressed:

David T. Wang
Department of Earth, Atmospheric, and Planetary Sciences
Massachusetts Institute of Technology
77 Massachusetts Ave, Bldg. E25-645, Cambridge, MA 02139, USA.
+1 (617) 324-3949
dtw@mit.edu

McB-13CH3D_Revised_v3b.docx

Abstract [max 500 words, ideally 200-300]

Aerobic oxidation of methane plays a major role in reducing the amount of methane emitted to the atmosphere from freshwater and marine settings. We cultured an aerobic methanotroph, *Methylococcus capsulatus* (Bath) at 30 and 37 °C, and determined the relative abundance of $^{12}CH_4$, $^{13}CH_4$, $^{12}CH_3D$, and $^{13}CH_3D$ (a doubly-substituted, or "clumped" isotopologue of methane) to characterize the clumped isotopologue effect associated with aerobic methane oxidation. In batch culture, the residual methane became enriched in ^{13}C and D relative to starting methane, with D/H fractionation a factor of 9.14 ($^{D}\varepsilon/^{13}\varepsilon$) larger than that of $^{13}C/^{12}C$. As oxidation progressed, the $\Delta^{13}CH_3D$ value of residual methane decreased. The isotopologue fractionation factor for $^{13}CH_3D$ was found to closely approximate that predicted by the product of the measured fractionation factors for $^{13}CH_4$ and $^{12}CH_3D$ (i.e., $^{13}C/^{12}C$ and D/H). The results give insight into enzymatic reversibility in the aerobic methane oxidation pathway. Based on the experimental data, a mathematical model was developed to predict isotopologue signatures expected for methane in the environment that has been partially-oxidized by aerobic methanotrophy. Measurement of methane clumped isotopologue abundances can be used to distinguish between aerobic methane oxidation and alternative methane-cycling processes. [204 words]

1. INTRODUCTION

Methane is an important long lived (well-mixed) greenhouse gas whose atmospheric concentration has more than doubled (~720 ppb to >1800 ppb) since pre-industrial time (Wahlen, 1993; IPCC, 2013). Important sources of atmospheric methane include natural wetlands (up to one-third of emissions), agriculture (including paddy rice fields and ruminant animals), and fossil fuel usage (Bousquet et al., 2006; Dlugokencky et al., 2011). Methanogenic archaea are responsible for the majority of emissions, with thermogenic sources accounting for most of the remainder. The primary methane sink in the atmosphere is reaction with tropospheric hydroxyl radicals (OH). Despite rigorous bottom-up accounting and top-down estimates based on remote sensing data and high-frequency measurements, the flux of methane from sources and to sinks remains poorly constrained (e.g., Kirschke et al., 2013).

Emissions from natural and human-made wetlands and other aquatic environments account for nearly two-thirds of all methane sources, though substantial uncertainty is associated with source strength estimates (Kirschke et al., 2013). Methanotrophic processes consume over half of the methane produced in aquatic environments prior to emission into the atmosphere (Reeburgh, 2007). It is estimated that a large fraction of methane produced in freshwater sediments, as much as 90% at some sites (Oremland and Culbertson, 1992), is removed via the aerobic oxidation of methane. In addition, soil-dwelling aerobic methanotrophs are responsible for oxidation of a small fraction (~2%) of methane from the atmosphere (Kirschke et al., 2013). Furthermore, activity of methanotrophic bacteria with high affinity for atmospheric methane in Arctic soils has been reported (Lau et al., 2015). Thus, understanding the magnitude and dynamics of methanotrophic sinks is important for global methane cycle budgets and constraining inputs to climate simulations.

The bacterium *Methylococcus capsulatus* (Bath), an obligate aerobic methanotroph, is a model organism for studies of the genetics, physiology, and geomicrobiology of aerobic methane oxidation in sediments and water columns (Whittenbury et al., 1970; Bowman, 2014). This organism uses the enzymes soluble methane monooxygenase (sMMO) and particulate methane monooxygenase (pMMO) to oxidize methane to methanol, which is further oxidized to CO_2 as an end product (Hanson and Hanson, 1996). Carbon derived from methane can also be assimilated into cellular biomass. The overall reaction is thus described by the stoichiometry:

$$CH_4 + 2O_2 \rightarrow b\, C_{cell} + (1 - b)\, CO_2 + 2H_2O \quad (1)$$

where C_{cell} represents cellular carbon and b is the fraction of carbon assimilated into biomass.

In experiments with pure and enrichment cultures, microbes utilizing this pathway have been shown to generate large and correlated carbon ($^{13}C/^{12}C$) and hydrogen (D/H) isotope fractionations during aerobic methane oxidation (Coleman et al., 1981; Kinnaman et al., 2007; Powelson et al., 2007; Feisthauer et al., 2011). Measurements of $^{13}C/^{12}C$ and D/H ratios in environmental methane samples can be used to assess whether they have experienced partial oxidation (Hornibrook et al., 1997; Chanton et al., 2005).

Recently, methods were developed to determine the abundance of multiply-substituted "clumped" isotopologues (e.g., $^{13}CH_3D$) in methane samples to sub-permille precision (Ono et al., 2014; Stolper et al., 2014b; Young et al., 2016). Measurements of the abundance of multiply-substituted isotopologues are of geochemical interest because of their potential for use as an isotopic geothermometer that can be accessed via analyses of a single compound (Wang et al., 2004; Eiler, 2007). Furthermore, clumped isotopologue data provide another dimension for probing kinetic and equilibrium isotope effects and for constraining isotope exchange processes in natural settings (e.g., Eiler and Schauble, 2004, Yeung et al., 2012, and Yeung, 2016). For example, the isotope exchange reaction

$$^{13}CH_4 + {}^{12}CH_3D \rightleftharpoons {}^{13}CH_3D + {}^{12}CH_4 \quad (2)$$

has an equilibrium constant K that varies between ~1.007 at 0 °C to 1.000 at temperatures approaching infinity (at which isotopes are randomly distributed amongst all possible isotopologues, i.e., the stochastic distribution) (see Wang et al., 2015, and references therein for details regarding calculations from which K is obtained).

Subsequent surveys of methane in the environment revealed that in methane of microbial origin produced in both natural settings and pure cultures, the reaction quotient (Q, see also Sec. 2.2) of Reaction 2 varies between 0.997 and 1.007 (Stolper et al., 2014a; Inagaki et al., 2015; Stolper et al., 2015; Wang et al., 2015; Douglas et al., 2016), a range that is much larger than that expected for thermodynamic equilibrium (ca. 1.004 to 1.007) at temperatures at which microbial life is possible (~0 to 120 °C) (Wang et al., 2015). The nonequilibrium isotope signatures were attributed to intrinsic clumped isotopologue effects expressed during biological methanogenesis under conditions of low reversibility (Stolper et al., 2015; Wang et al., 2015). Using inferences based on $\delta^{13}C$ and δD data, methane oxidation was excluded as a significant origin of the nonequilibrium isotope signals (Wang et al., 2015). However, experimental constraints on the fractionation of $^{13}CH_3D$ during biological methane oxidation are lacking in the clumped isotope literature.

In this paper, we report experimental measurements of the fractionation of $^{13}CH_3D$ during aerobic methane oxidation by cultures of the bacterium *Methylococcus capsulatus* (Bath). It is demonstrated that aerobic methanotrophy affects the abundance of $^{13}CH_3D$ in a nonlinear fashion relative to $\delta^{13}C$ and δD; the directionality and magnitude of these effects depend on whether oxidation occurs in a closed or open system. We present simple models to illustrate the expected shifts in $^{13}CH_3D$ abundance under different scenarios, and review available environmental clumped isotopologue data in light of the new experimental constraints.

2. METHODS

2.1. Cultures

Methylococcus capsulatus strain Bath cultures were grown in 10 ml of nitrate mineral salts medium supplemented with 5 µM $CuSO_4$ (Welander and Summons, 2012). Serum bottles (160 cm^3) were inoculated with 2%(v/v) inoculum from a starter culture that had grown for ca. 30 hours, stoppered and sealed without removing ambient air, and injected with 20 cm^3 SATP (~810 µmol) of methane from commercially-sourced cylinders using a gas-tight syringe. Tests indicated that the starting gas compositions were consistent within analytical error (±5%) between serum bottles. Multiple serum bottles were inoculated for each of the two experimental temperatures (Table 1). Cultures were incubated at 30 or 37 °C while shaking at 225 rpm and sacrificed at given times by adding 1 ml of 1 M hydrochloric acid. Each row in Table 1 shows the composition of one serum bottle at the time at which the experiment was stopped. Experimental timepoints were selected based on monitoring of growth during preliminary incubations of starter cultures (by tracking optical density, see Supplementary Fig. 1). However, to minimize puncturing of the serum bottles during the isotopic fractionation experiments, optical densities were not measured for the samples for isotopologue analysis shown in Table 1. The combination of constant agitation, a large headspace volume relative to liquid volume, and high initial CH_4 partial pressures (>0.1 atm) ensures that diffusion into the liquid from the headspace does not limit the rate of methane consumption (Templeton et al., 2006; Nihous, 2008).

2.2. Analytical techniques

Concentrations of headspace gases, including CH_4 and CO_2, were determined via gas chromatography (GC) using a Shimadzu GC-2014 gas chromatograph configured with a packed column (Carboxen-1000, 5'× 1/8", Supelco, Bellefonte, Pennsylvania, USA) held at 140 °C and argon carrier gas, and thermal conductivity and methanizer-flame ionization detectors. Subsamples of the headspace (0.20 cm^3 at laboratory temperature, ~23 °C) from each serum bottle were taken via a gas-tight syringe and injected onto the column. Gas concentrations were determined directly as partial pressures. Accuracy of the analyses, evaluated from standards, was ±5%. The fraction of initial methane remaining, *f*, in each batch culture was calculated from these measurements (Table 1), with uncertainties propagated following Ku (1969).

Samples of methane were purified via cryofocusing–preparative gas chromatography through a packed column (Carboxen-1000, 5'× 1/8", Supelco) held at 30 °C with helium carrier gas, and cryotrapping of the eluted methane on activated charcoal at liquid nitrogen temperature (Wang et al., 2015). The relative abundances of the methane stable isotopologues $^{12}CH_4$, $^{13}CH_4$, $^{12}CH_3D$, and $^{13}CH_3D$ were measured using a tunable infrared laser direct absorption spectroscopy technique described previously (Ono et al., 2014; Wang et al., 2015).

Isotope values are reported herein using standard delta-notation.[1] In accordance with IUPAC recommendations (Coplen, 2011), we have omitted the factor of 1000‰ from the definition of δ and other isotope values (including $\Delta^{13}CH_3D$, below). Carbon and hydrogen isotope values were calibrated against community reference materials NGS-1 and NGS-3 (Wang et al., 2015).

The abundance of $^{13}CH_3D$ is tracked via the $\Delta^{13}CH_3D$ value, defined according to Ono et al. (2014) as:

$$\Delta^{13}\mathrm{CH_3D} = \ln Q, \text{ where } Q = \frac{[^{13}\mathrm{CH_3D}][^{12}\mathrm{CH_4}]}{[^{13}\mathrm{CH_4}][^{12}\mathrm{CH_3D}]} \qquad (3)$$

Here, Q is the reaction quotient for Reaction 2, and $\Delta^{13}CH_3D \approx Q - 1$ because Q is close to unity in the natural and experimental systems studied herein.[2] For a methane sample that has attained a distribution of isotopes among all isotopologues consistent with equilibrium at a given temperature, $Q = K$. The temperature dependence of the equilibrium $\Delta^{13}CH_3D$ value was theoretically estimated and experimentally calibrated previously (Wang et al., 2015).

Methane samples with a wide range of δD values (ca. −480‰ to +500‰ vs. SMOW) were prepared and thermally-equilibrated over platinum catalyst at 300 °C to correct for the nonlinearity in the spectroscopic analysis described by Ono et al. (2014).

2.3. Calculation of isotope and isotopologue fractionation factors

The MMO-catalyzed reaction between methane and O_2 to produce the intermediate product methanol is the first in a sequence of enzymatic reactions involved in aerobic methanotrophy (Sirajuddin and Rosenzweig, 2015). We focus on this reaction because it is the most important isotopically-fractionating step in this sequence as it is considered to be both rate-limiting and isotope-sensitive (Nesheim and Lipscomb, 1996) under the studied experimental conditions. Limitation of the rate of methane consumption by this step requires that methane

[1] Definitions: $\delta^{13}C = (^{13}C/^{12}C)_{sample}/(^{13}C/^{12}C)_{PDB} - 1$, and $\delta D = (D/H)_{sample}/(D/H)_{SMOW} - 1$ [for natural methane samples: $\delta^{13}C = (^{13}CH_4/^{12}CH_4)_{sample}/(^{13}C/^{12}C)_{PDB} - 1$ and $\delta D = ¼\ (^{12}CH_3D/^{12}CH_4)_{sample}/(D/H)_{SMOW} - 1$].

[2] From the approximation $\ln(1 + x) \approx x$ for values of x close to zero.

diffusion into and out of the cells be rapid relative to MMO catalysis. Following Nihous (2010), we assume that isotopic fractionation associated with transfer of methane across cell membranes is negligible.

The reaction scheme for the first step of the aerobic oxidation of the methane isotopologues $^{12}CH_4$, $^{13}CH_4$, $^{12}CH_3D$, and $^{13}CH_3D$ can be described by the following six chemical reactions:

$$^{12}CH_4 \longrightarrow {}^{12}CH_3OH \quad (4)$$

$$^{13}CH_4 \longrightarrow {}^{13}CH_3OH \quad (5)$$

$$^{12}CH_3D \longrightarrow {}^{12}CH_3OH \quad (6)$$

$$^{12}CH_3D \longrightarrow {}^{12}CH_2DOH \quad (7)$$

$$^{13}CH_3D \longrightarrow {}^{13}CH_3OH \quad (8)$$

$$^{13}CH_3D \longrightarrow {}^{13}CH_2DOH \quad (9)$$

2.3.1. Carbon isotope fractionation

Assuming that the reaction is irreversible, follows first-order kinetics, and occurs in a closed system, the following differential equations can be written for $^{12}CH_4$ and $^{13}CH_4$:

$$\frac{d\,[^{12}CH_4]}{dt} = -k \cdot [^{12}CH_4] \quad (10)$$

$$\frac{d\,[^{13}CH_4]}{dt} = -{}^{13}\alpha \cdot k \cdot [^{13}CH_4] \quad (11)$$

where k is the rate constant for $^{12}CH_4$ consumption (Reaction 4), and $^{13}\alpha$ is the fractionation factor for $^{13}C/^{12}C$ (ratio of rate constants for Reactions 5 and 4).

Combining Eqns. 10 and 11, eliminating dt, and integrating from $f = 1$ (initial) to f yields the equation:

$$\ln\left(\frac{[^{13}CH_4]_f}{[^{13}CH_4]_{\text{init}}}\right) = {}^{13}\alpha \cdot \ln\left(\frac{[^{12}CH_4]_f}{[^{12}CH_4]_{\text{init}}}\right) \quad (12)$$

Subtracting $\ln\left([^{12}CH_4]_f/[^{12}CH_4]_{\text{init}}\right)$ from each side, and using the approximations $f \approx [^{12}CH_4]_f/[^{12}CH_4]_{\text{init}}$ and $[^{13}CH_4]/[^{12}CH_4] \approx [^{13}C]/[^{12}C]$, a form of the classic "Rayleigh equation" is obtained (Mariotti et al., 1981):

$$\ln\frac{\delta^{13}C+1}{\delta^{13}C_{\text{init}}+1} = \left({}^{13}\alpha - 1\right)\ln f \quad (13)$$

2.3.2. Hydrogen isotope fractionation

For the D-substituted isotopologue $^{12}CH_3D$, there are two ways to break a carbon-hydrogen bond. These two pathways are described by Reactions 6 and 7. The former involves the breakage of the C–D bond (accompanied by a primary isotope effect, described by the fractionation factor $^{D}\alpha_p$), while the latter involves the breakage of any of the three C–H bonds *adjacent* to the C–D bond (incurring a secondary isotope effect, $^{D}\alpha_s$). Thus, the overall rate of the oxidation of $^{12}CH_3D$ to methanol can be described by:

$$\frac{d^{12}\mathrm{CH_3D}}{dt} = -\frac{1}{4}\cdot\ {}^{\mathrm{D}}\alpha_{\mathrm{p}}\cdot k\cdot\left[{}^{12}\mathrm{CH_3D}\right] - \frac{3}{4}\cdot\ {}^{\mathrm{D}}\alpha_{\mathrm{s}}\cdot k\cdot\left[{}^{12}\mathrm{CH_3D}\right] \quad (14)$$

By lumping together ${}^{\mathrm{D}}\alpha_{\mathrm{p}}$ and ${}^{\mathrm{D}}\alpha_{\mathrm{s}}$, the rate equation can be simplified to:

$$\frac{d^{12}\mathrm{CH_3D}}{dt} = -\ {}^{\mathrm{D}}\alpha\cdot k\cdot\left[{}^{12}\mathrm{CH_3D}\right], \quad (15)$$

where ${}^{\mathrm{D}}\alpha = \frac{1}{4}\,{}^{\mathrm{D}}\alpha_{\mathrm{p}} + \frac{3}{4}\,{}^{\mathrm{D}}\alpha_{\mathrm{s}}$.

This parameterization of D/H fractionation is attractive in that it allows for apparent overall isotopic fractionation factors to be constrained by cell culture experiments and measurement with conventional geochemical techniques (e.g., isotope ratio mass spectrometry), without measurement of the individual reaction products. Applying the same logic used in Sec. 2.3.1, the following expression is obtained:

$$\ln\frac{\delta\mathrm{D}+1}{\delta\mathrm{D_{init}}+1} = \left({}^{\mathrm{D}}\alpha - 1\right)\ln f \quad (16)$$

Combining Eqns. 13 and 16 yields an equation describing the correlation between carbon and hydrogen isotope fractionation:

$$\ln\frac{\delta\mathrm{D}+1}{\delta\mathrm{D_{init}}+1} = \left(\frac{{}^{\mathrm{D}}\alpha-1}{{}^{13}\alpha-1}\right)\ln\frac{\delta^{13}\mathrm{C}+1}{\delta^{13}\mathrm{C_{init}}+1} \quad (17)$$

2.3.3. $^{13}CH_3D$ fractionation

The rate of oxidation of $^{13}CH_3D$ can be described by:

$$\frac{d^{13}\mathrm{CH_3D}}{dt} = -\frac{1}{4}\cdot\gamma_{\mathrm{p}}\cdot\ {}^{13}\alpha\cdot\ {}^{\mathrm{D}}\alpha_{\mathrm{p}}\cdot k\cdot\left[{}^{13}\mathrm{CH_3D}\right] - \frac{3}{4}\cdot\gamma_{\mathrm{s}}\cdot\ {}^{13}\alpha\cdot\ {}^{\mathrm{D}}\alpha_{\mathrm{s}}\cdot k\cdot\left[{}^{13}\mathrm{CH_3D}\right] \quad (18)$$

Here, we have introduced the terms γ_p and γ_s to characterize deviations of the clumped isotopologue fractionation factor from the product of the $^{13}C/^{12}C$ and D/H fractionation factors (α values). When there is no deviation from this product (i.e., primary and secondary isotope fractionation factors for bond breakage in $^{13}CH_3D$ follow what is referred to hereafter as the "product rule"), both γ_p and γ_s are unity. Deviations from the product rule represent a "clumped isotopologue effect" on bond breakage that arises from the substitution of both ^{13}C and D in the substrate methane. To simplify the treatment of clumped isotopologue effects in the absence of literature data for γ_p and γ_s, we adopt the following form of the rate equation:

$$\frac{d^{13}\mathrm{CH_3D}}{dt} = -\gamma\cdot\ {}^{13}\alpha\cdot\ {}^{\mathrm{D}}\alpha\cdot k\cdot\left[{}^{13}\mathrm{CH_3D}\right] \quad (19)$$

Here, the "gamma-factor" (γ) is an empirically-constrained term that describes an *effective* clumped isotopologue fractionation factor. Implicit in the use of Eqn. 19 is that $\gamma\cdot\ {}^{\mathrm{D}}\alpha = \frac{1}{4}\cdot\gamma_{\mathrm{p}}\cdot\ {}^{\mathrm{D}}\alpha_{\mathrm{p}} + \frac{3}{4}\cdot\gamma_{\mathrm{s}}\cdot\ {}^{\mathrm{D}}\alpha_{\mathrm{s}}$ (from the definition of ${}^{\mathrm{D}}\alpha$ in Sec. 2.3.2; also see discussion in Sec. 4.1.2). This condition is satisfied, although not uniquely, when γ is equal to both γ_p and γ_s.

Equation 19 is convenient because it allows for γ to be constrained by measurements of the methane isotopologues in experiments conducted at natural abundance without the use of isotopically labeled substrates or measurement of individual isotopically-substituted products. Integration of Eqn. 19 combined with Eqn. 10,

subtraction of the isotopologue-ratio forms of Eqns. 13 and 16 from the result, and substitution of the definition of $\Delta^{13}CH_3D$ (Eqn. 3) yields:

$$\Delta^{13}CH_3D = \Delta^{13}CH_3D_{initial} + \left(\gamma \cdot {}^{13}\alpha \cdot {}^{D}\alpha - {}^{13}\alpha - {}^{D}\alpha + 1\right) \cdot \ln f \quad (20)$$

By adopting this greatly simplified treatment, it necessarily means that differences in primary and secondary isotope effects for different forms of the enzyme in different methanotroph species are masked and lumped into an "effective" fractionation factor. A similar line of reasoning was used by Stolper et al. (2015) to simplify the representation of a model methanogenic system.

3. RESULTS

During the course of the experiments at 30 and 37 °C, the concentration of methane in the headspace decreased and the concentration of CO_2 increased (Table 1). The bottles incubated at 37 °C exhibited a lag phase (observed in preliminary experiments with starter cultures), with a rapid transition into active methane consumption around 41 hours after inoculation, whereas in the 30 °C experiments, methane consumption began immediately after inoculation, but at an apparently lower rate (Table 1 and Supplementary Fig. 1). Based on mass balance of measured CO_2 and CH_4 concentrations relative to initial CH_4 (Table 1), ~7% to 41% of carbon was not accounted for; this fraction of carbon was likely incorporated into cellular biomass (*b* in Eqn. 1). This range of *b* values is similar to ranges observed in previous studies (e.g., 0.1−0.5 in Templeton et al., 2006).

The initial isotopic composition of the methane used was different between the two sets of experiments (Table 1). As methane was consumed, the $\delta^{13}C$ and δD values of the residual methane increased (Fig. 1), indicating a preferential consumption of the lighter ^{12}C and ^{1}H by the bacteria. Conversely, $\Delta^{13}CH_3D$ values of the residual methane decreased as methane was consumed, starting from initial values of ca. +2.6‰ and +2.2‰, and decreasing to "anticlumped" (<0‰) values of ca. −1.5‰ and −1.9‰, respectively, at the last time points sampled in the 30 and 37 °C experiments (Table 1).

Using Eqns. 13, 16, and 20, values of the fractionation factors ${}^{13}\alpha$, ${}^{D}\alpha$, and γ were calculated for each time point after the initial (Table 1). All calculations used the initial timepoint as the reference starting point; thus, the fractionation factors reported are averaged over the entire reaction occurring in the bottle, and contain correlated errors linked to the uncertainty in data from the initial timepoint. Fractionation factors were calculated for each timepoint, rather than over all bottles in an experiment, to avoid artifacts from variable growth between bottles, particularly at the lower temperature of 30 °C (see Supplementary Fig. 1). In the earlier time points, the error in the calculated fractionation factors is large because of uncertainties in *f* and in $\Delta^{13}CH_3D$. For each set of experiments, the weighted-averages of the fractionation factors were determined, and are listed in Table 1, and the corresponding trajectories (using experimental ${}^{13}\alpha$ and ${}^{D}\alpha$ values, and variable γ) are depicted in Fig. 1.

Isotopic fractionation of D/H was substantially greater in magnitude than that of $^{13}C/^{12}C$ (Fig. 2a). In general, a greater degree of both carbon- and hydrogen-isotope fractionation was observed in the bottles incubated at 37 °C than at 30 °C (Fig. 2b). No systematic changes in the magnitude of isotope fractionation were observed over the course of the experiments (Table 1). A similar, tight correlation of D/H and $^{13}C/^{12}C$ fractionation is observed between the two sets of experiments (Fig. 2a).

Calculated γ values for each experimental timepoint are shown in Table 1. All values were close to unity, and showed no systematic changes over the course of incubation. The weighted-average γ values for the experiments

were identical to unity within 2σ error (1.0005 ± 0.0006 and 1.0000 ± 0.0014 for the 30 and 37 °C experiments, respectively).

4. DISCUSSION

4.1. Isotope and isotopologue fractionation during aerobic methanotrophy

4.1.1. Fractionation of methane $^{13}C/^{12}C$ and D/H ratios

A wide range of carbon isotope fractionation factors ($^{13}\varepsilon$ ranging from −38‰ to −3‰) have been reported in culture- and field-based studies [see Templeton et al. (2006) and references therein]. The variable nature of the magnitude of observed carbon isotope effects complicates application of measurements of individual carbon isotope ratios in diagnosing the presence and extent of methanotrophy in the environment. As such, the use of paired $\delta^{13}C$ and δD data has been suggested as a possible method of removing some levels of ambiguity associated with the sole use of carbon-isotopes (Elsner et al., 2005). Although the absolute magnitudes of isotope fractionation may vary due to "masking effects" from preceding isotopically-insensitive steps such as transport across membranes or binding to an enzyme (Feisthauer et al., 2011), a correlation between the fractionation of the carbon and hydrogen isotopes can be expected because both are principally influenced by the breakage of the C–H bond. Such a correlation was first noted by Coleman et al. (1981), with later studies (Kinnaman et al., 2007; Powelson et al., 2007; Feisthauer et al., 2011) corroborating the observations in pure culture and in enrichments from other environments. The published values of $^{D}\varepsilon/^{13}\varepsilon$, corresponding to the slope of the gray lines in Fig. 2a, range from 5.9 to 14.9, with a mean of 8.9 ± 2.3 [standard deviation (1*s*), $n = 15$]. The best-fit value of $^{D}\varepsilon/^{13}\varepsilon$ for the data shown in Table 1 is 9.14, a value which appears independent of the two growth temperatures tested, and which falls near the middle of the published range.

The consistency of the determined $^{D}\varepsilon/^{13}\varepsilon$ ratios with those in the literature provides confidence that results regarding the behavior of $\Delta^{13}CH_3D$ (discussed below) during aerobic methane oxidation by *M. capsulatus* (Bath) can be generalizable to other strains grown under other conditions. Further experiments with these strains grown under different conditions to examine clumped isotopologue fractionation will help to determine if this hypothesis is valid. In a previous study, various strains of bacteria [including *M. capsulatus*, which has two pMMOs and one sMMO (Ward et al., 2004)] grown in batch cultures under different copper (Cu) concentrations (with pMMO expressed under Cu-rich conditions and sMMO under low Cu) demonstrated consistently correlated fractionations of carbon and hydrogen isotopes, without apparent correlation to physiology or growth condition (Feisthauer et al., 2011). Values of $^{D}\varepsilon/^{13}\varepsilon$ derived from that study range from 7.3 to 8.8, and are close to the average $^{D}\varepsilon/^{13}\varepsilon$ ratio from our dataset (9.14, Fig. 2a). In particular, *M. capsulatus* grown at 45 °C induced isotopic fractionations of $^{13}\alpha = 0.972 \pm 0.002$ and $^{D}\alpha = 0.769 \pm 0.030$ (published uncertainties were listed as 95% confidence interval, approximately 2σ) under Cu-rich conditions, and under Cu-poor conditions, similar values of $^{13}\alpha = 0.977 \pm 0.003$ and $^{D}\alpha = 0.808 \pm 0.029$ (Feisthauer et al., 2011). The corresponding $^{D}\varepsilon/^{13}\varepsilon$ ratios (with propagated ~2σ uncertainties) indicated by their data are 8.3 ± 1.1 and 8.4 ± 1.7 under Cu-rich and Cu-poor conditions, respectively. These values are indistinguishable from the $^{D}\varepsilon/^{13}\varepsilon$ ratio derived from regression through our experimental data (9.14 ± 0.14, 2σ; see Table 2). This correspondence of $^{D}\varepsilon/^{13}\varepsilon$ ratios suggests that the proposed product rule for γ values (see Sec. 4.1.2) could be valid for *M. capsulatus* expressing either pMMO or sMMO, and may hold for many other methanotrophic strains cultured under various conditions.

Insights into the origin of D/H fractionation during methane oxidation have been obtained from studies which separately constrain the primary and secondary hydrogen isotope effects. Using molecular dynamics simulations, Pudzianowski and Loew (1983) calculated the intermolecular and intramolecular isotope effects associated with the abstraction of H or D from CH_4 or CH_3D by atomic oxygen, $O(^3P)$, as an analog for the methane monooxygenase reaction. Their results, expressed as fractionation factors, are ${}^{D}\alpha_p = 0.0296$ and ${}^{D}\alpha_s = 0.763$ (or 0.0179 and 0.759 when tunneling corrections were applied). Thus, the overall isotope fractionation, ${}^{D}\alpha$ (see Eqn. 15), would be 0.580. This fractionation factor reflects a much larger magnitude of D/H fractionation than is observed in either our experiments (${}^{D}\alpha$ as low as 0.718) or those reported in other studies (plotted in Fig. 2b). Pudzianowski and Loew (1983) note, however, that the transition state of the $CH_4/CH_3D + O(^3P)$ reaction they modeled has only qualitative similarity to the transition state of the methane hydrogen abstraction/hydroxylation reaction performed by methane monooxygenase. Such fundamental differences between the two processes may explain the difference between their calculated fractionation and the experimental observations.

Multiple experimental determinations of the intermolecular and intramolecular kinetic isotope effects for H or D abstraction have been reported [e.g., Green and Dalton (1989), Rataj et al. (1991) and Wilkins et al. (1994), and references therein]. Values for the primary isotope effect (corresponding to ${}^{D}\alpha_p = 0.73$) and secondary isotope effect (${}^{D}\alpha_s = 0.93$) have been reported for methane oxidation by sMMO (Wilkins et al., 1994). The overall ${}^{D}\alpha$ calculated from these values (0.88 via Eqn. 15) is not low enough to explain the observed D/H fractionations in culture (Fig. 2b). More recently, in experiments with a series of multiply-deuterated isotopologues of methane, Nesheim and Lipscomb (1996) determined that the isotopically-selective reaction of compound Q (the key intermediate that oxidizes CH_4) of the MMO hydroxylase ($MMOH_Q$) has very large primary and much smaller secondary kinetic isotope effects corresponding to ${}^{D}\alpha_p = 0.01–0.02$ and ${}^{D}\alpha_s = 0.9–1.0$. Via Eqn. 15, the corresponding overall hydrogen isotope fractionation, ${}^{D}\alpha$, is then between ~0.68 and ~0.76, a range which overlaps with the largest D/H fractionation observed in our experiments (0.718, Table 1). Note that such a direct quantitative comparison between isotope effects determined from pure cultures and those from *in vitro* experiments with labeled substrates may not be meaningful, as in culture experiments the fractionation induced by MMO is not necessarily the only factor determining isotopic fractionation. Regardless, the very large primary kinetic isotope effect implies that nearly all of the $^{12}CH_3D$ reacts via the abstraction of H, with only a minor fraction reacting via the abstraction of D. This inference has potential implications for the interpretation of γ factors constrained by clumped isotopologue measurements (see Sec. 4.1.2).

Generally larger bulk carbon and hydrogen isotopic fractionations were observed in the 37 °C cultures, compared to those grown at 30 °C (Table 1). This trend is an apparent reversal of the normally-expected decrease of kinetic isotope effects with increasing temperature. Such an inverse temperature effect was previously observed by Coleman et al. (1981) on enrichment cultures grown at 11.5 and 26 °C. They excluded species differences as the source of the apparent trend, and speculated that the partial and differential expression of a combination of kinetic and equilibrium isotope effects could explain their results.

In our experiments, only one strain of bacterium was cultured, thus also excluding species differences as a reason for the observed inverse temperature trend. If some D/H exchange with cellular water occurs during C–H bond breakage and re-forming, the overall ${}^{D}\varepsilon$ fractionation factor should be of smaller magnitude than would otherwise be expected given the observed ${}^{13}\varepsilon$ value (as the carbon does not exchange). [The δD of water used in the cultures was not measured, but is estimated to be between −95‰ and −32‰ based on tap water data from Bowen et al.

(2007). Based on the calibration of Horibe and Craig (1995),[3] methane at D/H equilibrium with water at 30–37 °C would be expected to have $\delta D < -200‰$, which is lower than the initial δD of methane in both sets of experiments.] The observation that the ratio $^{D}\varepsilon/^{13}\varepsilon$ is nearly identical between the two temperatures (Fig. 2a) therefore argues against C–H bond re-equilibration as an explanation for smaller magnitudes of isotopic fractionation in the 30 °C experiments. Furthermore, our additional measurements of $\Delta^{13}CH_3D$ indicate that γ values are indistinguishable (within 2σ, Table 1) between the two experiments, lending additional support to the conclusion that kinetic isotope fractionation dominates the observed isotope and isotopologue signals.

Given the above analysis, an alternate explanation must be sought to explain the observed apparent inverse temperature trend. According to the theory of kinetic isotope fractionation (e.g., Bigeleisen, 1949), predictions of decreasing kinetic isotope effects with increasing temperature are generally valid only for elementary reactions. The aerobic oxidation of methane by *M. capsulatus* consists of multiple enzymatic steps, and thus expression of intrinsic kinetic isotope effects may not be complete if the isotopically-sensitive methane monooxygenase reaction is not fully rate-limiting. In particular, models proposed to explain previously published experimental data point to the depletion of soluble methane concentrations below threshold levels required to maintain rates of mass transfer into the cell as a control on the degree to which kinetic isotope effects are expressed in culture (Nihous, 2008; Nihous, 2010; Vavilin et al., 2015). This behavior is analogous to that observed for $^{34}S/^{32}S$ ratios during microbial sulfate reduction, where under low sulfate conditions, sulfur isotope fractionation is suppressed due to rate limitation by the isotopically-insensitive initial transport of sulfate into the cell (Harrison and Thode, 1958; Rees, 1973). Substrate limitation has also been considered to explain trends associated with $^{13}C/^{12}C$ fractionation during methanogenesis under low intracellular CO_2 levels (e.g., Valentine et al., 2004), and has been extensively studied in relation to CO_2 levels during photosynthesis (e.g., Farquhar et al., 1982). Thus, the apparent inverse temperature trend in the data is possibly a result of masking of intrinsic isotope effects of MMO due to limitation from mass transport into the cell, although other explanations cannot be discounted. Experimental setups that allow rigorous accounting of carbon budgets and biomass density may allow for quantitative models of isotopologue systematics, similar to those created for $\delta^{13}C$ (Templeton et al., 2006; Nihous, 2008; Nihous, 2010), to be used in evaluating the potential effects of diffusion of methane to and through cells. Our data thus also encourages consideration of mass transport and bioavailable methane levels when evaluating methane isotope data in field settings where oxidation may be occurring. Despite the particular mechanisms underlying apparent inverse temperature trends remaining unclear, the general observation that the fractionation of $^{13}C/^{12}C$ and D/H ratios observed in our study is consistent with previously reported experiments is key, as it suggests that the discussion below regarding patterns of fractionation of $^{13}CH_3D$ may be generally applicable to experimental cultures of aerobic methanotrophic bacteria.

4.1.2. Fractionation of $^{13}CH_3D$

In our batch culture experiments, the $\Delta^{13}CH_3D$ value of residual methane decreased with progressive oxidation (Table 1). The weighted average γ values determined for the both the 30 °C experiment (1.0005 ± 0.0006, 2σ) and the 37 °C experiment (1.0000 ± 0.0014) are indistinguishable from unity. Thus, the results of this study indicate that the overall kinetic fractionation factor for $^{13}CH_3D$ can be closely approximated as the product of the carbon and hydrogen isotopic fractionation factors (i.e., $^{13\text{-}D}\alpha = {}^{13}\alpha \times {}^{D}\alpha$). This product rule can be used to model

[3] Comparisons of the fractionation factor for D/H equilibrium between $CH_4(g)$ and $H_2O(l)$ derived from the calibrations of different studies reveal a substantial range in estimates (up to 30‰ at 30–37 °C, see Wang et al., 2015). This is mainly due to uncertainty in extrapolations of experimental calibrations of $H_2(g)/H_2O(g)$ at >200 °C to lower temperatures. However, this level of uncertainty does not impact the interpretation developed here.

the $\Delta^{13}CH_3D$ value resulting from aerobic methane oxidation. If a higher level of prediction is necessary, precise constraints on primary and secondary α and γ values are required (see Sec. 2.3.3 and discussion below).

Given low enough γ values (depending on $^{13}\alpha$ and $^{D}\alpha$), the $\Delta^{13}CH_3D$ value may actually *increase* over the course of the reaction in a closed system such as a batch culture. The break-even condition, under which $\Delta^{13}CH_3D$ does not change over the course of a closed system process, occurs when $\gamma = \left(^{13}\alpha + {}^{D}\alpha - 1\right)/\left(^{13}\alpha \cdot {}^{D}\alpha\right)$. For the 30 and 37 °C experiments, the break-even γ values are 0.9986 and 0.9943, respectively. These values are substantially less than those determined experimentally above (the latter by a considerable −0.0057 or −5.7‰). Therefore, it should not be assumed that $\Delta^{13}CH_3D$ values are unaffected by closed system methane oxidation. Otherwise, the apparent $\Delta^{13}CH_3D$ temperature may be substantially overestimated or become imaginary, as shown in Fig. 3a.

There is no *a priori* reason that γ must be close to unity.[4] The γ factor as defined in Sec. 2.3.3 is empirically useful in that it is a single number that expresses the reactivity of $^{13}CH_3D$ relative to the other isotopologues. Because $^{13}CH_3D$ can react by two nonidentical hydrogen-abstraction reactions (Reactions 8 and 9), the γ value expresses the summation of the products of the hydrogen-isotope effects ($^{D}\alpha_p$ and $^{D}\alpha_s$) and the "clumped isotopologue effects" (γ_p and γ_s) for D in both primary and secondary sites: $\gamma \cdot {}^{D}\alpha = \frac{1}{4} \cdot \gamma_p \cdot {}^{D}\alpha_p + \frac{3}{4} \cdot \gamma_s \cdot {}^{D}\alpha_s$. A conceptual exercise helpfully illustrates the relative weighting of D- vs. H-abstraction reactions expressed in the γ factor. Assuming $^{D}\alpha_p = 0.02$ and $^{D}\alpha_s = 0.9$ (from Sec. 4.1.1), and $\gamma = 0.9990$ (i.e., −1‰ from unity, which is at the lower edge of 2σ uncertainty on the weighted average γ values for the experiments shown in Table 1), then $^{D}\alpha = 0.68$ and $0.6786 = 0.0050 \cdot \gamma_p + 0.6750 \cdot \gamma_s$. Assigning a value to either γ_p or γ_s would constrain the other; hence, two extreme cases can be considered: (*i*) if $\gamma_s = 1$, then $\gamma_p = 0.86$; or alternatively (*ii*) if $\gamma_p = 1$, then $\gamma_s = 0.9990$. The former case requires a large primary clumped isotopologue effect because proportionally very few $^{13}CH_3D$ (and $^{12}CH_3D$) molecules react through direct D-abstraction rather than H-abstraction (see Sec. 4.1.1), whereas the latter requires only a much smaller secondary clumped isotopologue effect on H-abstraction from $^{13}CH_3D$ to explain a γ value that deviates slightly from unity. Although insufficient constraints on either γ_p or γ_s are currently available, this exercise indicates that a small secondary clumped isotopologue effect (i.e., $\gamma_s \neq 1$ but is very close) could exist, but may be hardly detectable. Given the uncertainties surrounding experimental determinations of $^{D}\alpha_p$ and $^{D}\alpha_s$ (discussed in Sec. 4.1.1), accurate values of γ_p and γ_s cannot yet be assigned. For geochemical applications, the γ factor is at present best used as an empirically-fitted parameter, similar to the manner in which the overall D/H fractionation factor $^{D}\alpha$ is typically treated.

Irrespective of the exact magnitude of the γ factor, it is clear that $\Delta^{13}CH_3D$ becomes less clumped with progressive oxidation in a closed system under the growth conditions tested in this study. Because of the consistency of our $^{D}\varepsilon/^{13}\varepsilon$ results with previous experiments with organisms also using pMMO and/or sMMO (Fig. 2a), it is not unreasonable to expect similar results on $\Delta^{13}CH_3D$ values for methane oxidation by other strains of aerobic methanotrophic bacteria.

As mentioned above (Sec. 4.1.1), a possible explanation for the differences in the hydrogen isotopic fractionation factor for the experiments at the two temperatures relates to partial expression of equilibrium isotope effects in

[4] For example, when methane effuses through a small orifice, γ (when defined as the ratio of the isotopologue fractionation factor for $^{13}CH_3D/^{12}CH_4$ to the product of those for $^{13}CH_4/^{12}CH_4$ and $^{12}CH_3D/^{12}CH_4$) will not be unity. From the kinetic theory of gases, the rate of effusion of an isotopologue is proportional to $(\text{mass})^{-1/2}$, such that $\gamma = 1.00174$. Escaping methane will have lower (lighter) $\delta^{13}C$ and δD, but *higher* $\Delta^{13}CH_3D$, than the residual methane. For a more thorough discussion, readers are referred to Eiler and Schauble (2004).

one or both experiments. Evidence against this explanation derives from the observation that $\Delta^{13}CH_3D$ values of residual methane in both experiments follow the predictions of the product rule (i.e., γ values are ~1); therefore it is unlikely that there is a greater degree of C–H bond re-equilibration during the course of reaction in one experiment over another. Thus, clumped isotopologue data also assist in diagnosing presence or absence of isotope exchange during enzymatic abstraction of H from methane by MMO, and are consistent with a minor (not detectable) degree of reversibility for this process. The minor degree of reversibility indicated by the data for aerobic methane oxidation here contrasts sharply with the anaerobic oxidation of methane (AOM), an oxidation process in which much greater degrees of reversibility have been demonstrated using carbon and hydrogen isotopes (Holler et al., 2011; Yoshinaga et al., 2014). The environmental implications are discussed in Sec. 4.2.2.

4.2. Implications for biogeochemical systems

4.2.1. Methane isotope and isotopologue fractionation in open systems

In closed systems, e.g., batch cultures, no steady-state is obtained because of the lack of mass transfer to replenish the methane consumed by methane oxidation. However, in natural systems operating close to steady-state, there is replenishment of methane from lateral transport or diffusion, as well as methanogenesis, and there may be multiple sinks, including methane oxidation and mass transport (Fig. 4).

Experimental alternatives to batch cultures, namely flow-through bioreactors (chemostats), have been used to more directly approach the calibration of isotopic fractionation factors due to microbial metabolism in natural settings. For example, Templeton et al. (2006) grew pure and mixed cultures of aerobic methanotrophs in chemostats to determine the carbon isotope fractionation between methane and product methanol as a function of environmental and physiological conditions. In such an open system, there is a constant influx of reactant methane, which at steady-state is balanced by the sum of methane oxidation and methane carried in the effluent out of the bioreactor (i.e., dilution).

In the simple limiting case where the fraction of methane removed by oxidation approaches 100% (i.e., no methane escapes the system intact), there is effectively one sink of methane, with fractionation factors $^{13}\alpha$, $^{D}\alpha$, and γ accompanying the removal process. At steady state, the isotopic values of methane in the bioreactor would be $\delta^{13}C = (\delta^{13}C_{in} + 1) / {}^{13}\alpha - 1$ and $\delta D = (\delta D_{in} + 1) / {}^{D}\alpha - 1$, where δ_{in} represents the isotopic composition of the influent methane. For $^{13}CH_3D$, it can be shown that

$$\Delta^{13}CH_3D = \Delta^{13}CH_3D_{in} - \ln\gamma \qquad (21)$$

as presented in Joelsson et al. (2015). Since $\gamma \approx 1$, this expression can be approximated by $\Delta^{13}CH_3D = \Delta^{13}CH_3D_{in} - (\gamma - 1)$. In our batch culture experiments at 30 and 37 °C, respectively, weighted-average values for $(\gamma - 1)$ of +0.5 ± 0.3‰ and 0.0 ± 0.7‰ (1σ) were obtained (Table 1). Although steady-state experiments were not conducted in the current study, if it is assumed that these values are also characteristic of true open-system isotopologue fractionation factors, then the above expression can be used to place bounds on the isotopologue composition of methane in the limiting case outlined above. Examples of the calculated methane isotopic/isotopologue compositions are shown for model scenarios in Fig. 5a (corresponding to the endmember labeled “fully oxidative” on each curve).

Equation 21 also shows that in a system at steady-state where methane is solely removed by one process (here, oxidation), the $\Delta^{13}CH_3D$ value is determined solely by the $\Delta^{13}CH_3D$ value of the methane source and the γ factor, in contrast to closed systems where $\Delta^{13}CH_3D$ of residual methane is influenced also by the isotopic fractionations

for bulk $^{13}C/^{12}C$ and D/H. However, in more complex systems with multiple removal processes and associated fractionation factors, the partitioning of flows among the removal processes must be considered (Hayes, 2001).

One example of such an open system is shown in Fig. 4. Here, methane is carried into the system via advection, and removed by both advection and oxidation. Oxidation of methane has associated fractionation factors $^{13}\alpha$, $^{D}\alpha$, and γ, whereas transport processes are assumed to cause no fractionation (Alperin et al., 1988), i.e., values of α and γ are unity. The fraction of methane removed via oxidation, φ_{ox}, describes the partitioning of flows among the two methane sinks. It can be shown that at steady state, the hydrogen isotopic composition of the methane in the reservoir is (Hayes, 2001):

$$\delta D = \frac{\delta D_{in}+1}{1+\varphi_{ox}\left(^{D}\alpha-1\right)} - 1 \qquad (22)$$

An analogous equation (not shown) describes the carbon isotopic composition of methane in this system at steady state. When the $\delta^{13}C$ and δD values are plotted against each other, it can be seen that the trajectory describing the continuum between the fully-advective ($\varphi_{ox} = 0$) and fully-oxidative ($\varphi_{ox} = 1$) endmembers is slightly curved (though approximately linear at most scales of interest, Fig. 5b).

For this system, unlike in the simple fully-oxidative case described by Eqn. 21, the abundance is affected not only by the γ value, but also by the $^{13}\alpha$ and $^{D}\alpha$ values:

$$\Delta^{13}CH_3D = \Delta^{13}CH_3D_{in} - \ln\frac{1+\varphi_{ox}\left(\gamma\cdot{}^{13}\alpha\cdot{}^{D}\alpha-1\right)}{\left(1+\varphi_{ox}\left(^{13}\alpha-1\right)\right)\left(1+\varphi_{ox}\left(^{D}\alpha-1\right)\right)} \qquad (23)$$

This results in a parabolic curve connecting the fully-advective and fully-oxidative endmembers (Fig. 5a). For aerobic methane oxidation, the curvature on Fig. 5a is always expected to be concave up, because both the $^{13}\alpha$ and $^{D}\alpha$ values are less than unity. The relative position of the endmembers in $\Delta^{13}CH_3D$ space is determined by the γ value. When $\varphi_{ox} = 1$, Eqn. 23 reduces to Eqn. 21.

4.2.2. $\Delta^{13}CH_3D$ as an environmental tracer of methane sink processes

Both biological and chemical processes are important sinks in the methane budget. In terrestrial ecosystems and oxygenated marine water columns, aerobic methanotrophy dominates, whereas in sulfate-rich marine sediments and gas seeps, anaerobic consumption of methane becomes important (Cicerone and Oremland, 1988; Reeburgh, 2007; Valentine, 2011; Boetius and Wenzhöfer, 2013). In the atmosphere, the primary sink (~90%) is the reaction with tropospheric OH, with small contributions from microbial oxidation in soils, loss to stratosphere, and reaction with tropospheric Cl (Kirschke et al., 2013).

These methane-consuming processes impart distinct carbon- and hydrogen-isotopic fractionations. In general, biological processes (including aerobic methane oxidation, anaerobic oxidation of methane, and nitrite-dependent anaerobic methane oxidation) have $^{D}\varepsilon/^{13}\varepsilon$ ratios between 6 and 15, whereas the atmospheric sinks, CH_4 + OH and CH_4 + Cl, have $^{D}\varepsilon/^{13}\varepsilon$ ratios ~58 and ~5.5, respectively (Table 2). The consistent and sizable differences in isotopic behavior among the two atmospheric processes vs. biological processes is useful for constraining the balance of different sources and sinks of methane [e.g., (Whiticar and Schaefer, 2007; Kai et al., 2011; Rigby et al., 2012)].

The behavior of methane clumped isotopologues in atmospheric reactions has also been studied. Recently, Joelsson et al. (2014) and Joelsson et al. (2015) reported the fractionation factor for $^{13}CH_3D$ in relative-rate

experiments on the reactions of Cl and OH, respectively. Their experiments were conducted with mixtures of $^{12}CH_4$ and $^{13}CH_3D$ (and also $^{12}CH_3D$ in the OH study). Based on their measurements, the γ value associated with methane oxidation by Cl was 0.980 ± 0.019, and by OH was 0.978 ± 0.028 (2σ, Table 2). The γ value for Cl oxidation is slightly less than unity, implying that less of the $^{13}CH_3D$ is oxidized than would be predicted by the product rule, whereas the γ value for OH oxidation is within error of unity. However, the uncertainty on calculated γ values is large (ca. 20 to 30‰) due to limitations associated with the experimental setup and detection technique. Because $\Delta^{13}CH_3D$ in the environment has a ca. 10‰ range (Wang et al., 2015), more precise isotopologue-specific measurements of methane in experiments conducted at natural abundance will be necessary in order to constrain clumped isotopologue fractionations in atmospheric contexts. These experiments have been conducted, and the results are reported in a companion article (Whitehill et al., in revision); a summary of their results are shown in Table 2.

In the present study, γ values for aerobic methane oxidation were determined (1.0004 ± 0.0006, 2σ, Table 2). These values indicate that the abstraction of H from methane by methane monooxygenase is associated with little to no reversibility (see discussion in Sec. 4.1.2). This interpretation is consistent with the strong energetic favorability of methane oxidation to methanol and downstream products in the presence of abundant O_2, a strong electron acceptor (Cicerone and Oremland, 1988; Hanson and Hanson, 1996).

The new experimental constraints on clumped isotopologue fractionation during aerobic methane oxidation also afford an opportunity to briefly evaluate whether aerobic methane oxidation has influenced methane clumped isotopologue data available in the literature from various environments. In particular, because methane oxidation demonstrably produces nonequilibrium clumped isotopologue signatures in both closed and open systems considered in this study (Figs. 3 and 5, respectively), the out-of-equilibrium clumped isotopologue signatures in samples from Upper and Lower Mystic Lakes (Massachusetts, USA), Swamp Y (Massachusetts, USA), and The Cedars (California, USA) are considered again here (Wang et al., 2015), as well as a sample from a pond at Caltech for which a related parameter, the Δ_{18} value, was found to be in disequilibrium (Stolper et al., 2015). At Upper Mystic Lake (a 20-m deep seasonally-stratified freshwater lake), bubble traps were deployed ~2 m above the lake floor; the deployment of traps at such deep depths, into the oxygen-depleted hypolimnion (Peterson, 2005), was designed to minimize the possibility of aerobic methane oxidation (Wang et al., 2015). At Lower Mystic Lake (a 24-m deep meromictic density-stratified lake), the monimolimnion (from which the reported sample was taken) is anoxic (Wang et al., 2015), rendering aerobic methane oxidation unlikely. For Swamp Y and the Caltech pond, the redox state of the sediments from which the methane bubbles were stirred and extracted is unknown. At The Cedars, the extremely high levels of H_2 in gases exsolving from the springs maintains O_2 at vanishingly low levels (near the lower bound of H_2O stability, Morrill et al., 2013). Taken together, all methane samples from these four sites exhibit narrow ranges of $\delta^{13}C$ values between −59‰ and −71‰ and δD values between −265‰ and −342‰, but carry a wide range of nonequilibrium $\Delta^{13}CH_3D$ values (from −3.4‰ to +3.2‰) that are consistent within sites but significantly different between sites (Wang et al., 2015), and exhibit isotopologue patterns that do not discernably resemble those depicted in Figs. 3 and 5. Thus, although aerobic methane oxidation cannot be fully discounted at these four sites, the experimental constraints provided in the current study do not contraindicate the assumptions made by Wang et al. (2015) and are consistent with the hypothesis that nonequilibrium $\Delta^{13}CH_3D$ values in microbial methane in the environment and in methanogenic cultures studied to date originate primarily from intrinsic isotopologue effects during the assembly of C–H bonds during methanogenesis (Stolper et al., 2015; Wang et al., 2015).

Alternative biological mechanisms for methane oxidation are also important in the environment. Of particular interest is the sulfate-dependent anaerobic oxidation of methane (AOM), which is a major sink of methane in anoxic marine sediments (Reeburgh, 1976). This process operates via a very different biochemical pathway from that used by aerobic methanotrophs. While the biochemistry of AOM has not been fully characterized, it is likely that the enzymatic pathway of AOM is the reverse of methanogenesis, and involves the same or similar key enzymes (e.g., methyl-coenzyme M reductase) for addition or removal of H from single-carbon compounds (Scheller et al., 2010). Previously, it was found that as the reversibility of methanogenesis decreased (controlled in part by levels of bioavailable H_2), both the δD and $\Delta^{13}CH_3D$ values of the generated methane became lower or more negative (Wang et al., 2015); similar behavior was found in Δ_{18} (Stolper et al., 2014a; Stolper et al., 2015). From incubations of enrichment cultures of microbial consortia performing AOM, Holler et al. (2009) determined substantial kinetic isotope fractionations associated with this process ($^{13}\varepsilon = -12‰$ to $-36‰$ and $^{D}\varepsilon = -100‰$ to $-230‰$). The negative D/H fractionation factor results in the residual methane becoming enriched in D. Because of the demonstrated high levels of reversibility of AOM (Holler et al., 2011) and the re-equilibration of $^{13}C/^{12}C$ ratios between methane and inorganic carbon at the sulfate-methane transition zone (Yoshinaga et al., 2014), it seems reasonable to speculate that AOM may produce clumped isotope signatures distinct from those of methanogenesis (Stolper et al., 2015). In particular, the expression of a combination of kinetic and equilibrium isotope effects may be observed, such that the observed $\Delta^{13}CH_3D$ value may lie between that predicted by the product rule and that predicted for thermodynamic equilibrium. If so, then measurement of $\Delta^{13}CH_3D$ may provide a way to differentiate between AOM and aerobic methanotrophy. Alternatively, if AOM also generates $\Delta^{13}CH_3D$ approximating the product rule, then the agreement of $^{D}\varepsilon/^{13}\varepsilon$ between AOM (Holler et al., 2009) and aerobic methanotrophs (Table 2) suggests that potentially, microbially-mediated oxidation of methane produces only a small and predictable range of clumped isotopologue fractionations.

Another process, the recently-identified nitrite-dependent anaerobic methane oxidation (Ettwig et al., 2010), may also be environmentally-relevant, though its global prevalence has yet to be established. The bacterium Candidatus *Methylomirabilis oxyfera* produces molecular oxygen intracellularly from the reduction of nitrite to nitric oxide (Ettwig et al., 2010), in the absence of environmental O_2; the generated oxygen is then consumed along with methane by membrane-bound pMMO through the aerobic pathway. Because of the biochemical homology of the bond-breaking enzymatic step to that of aerobic methanotrophy, it is not unreasonable to expect that nitrite-dependent anaerobic methane oxidation would produce isotopic and clumped isotopologue patterns similar to those observed in this study. Indeed, carbon and hydrogen isotope fractionation factors for this process, as determined from culture experiments (Rasigraf et al., 2012), correlate in a manner that overlaps with aerobic methane oxidation (Table 2), lending support to this hypothesis.

5. CONCLUSIONS

Experimental investigation of the abundance of four methane stable isotopologues ($^{12}CH_4$, $^{13}CH_4$, $^{12}CH_3D$, and a clumped isotopologue, $^{13}CH_3D$) during oxidation of methane with O_2 by *Methylococcus capsulatus* (Bath) grown at 30 and 37 °C indicates that $\Delta^{13}CH_3D$ values of residual methane decrease systematically over the course of reaction in batch culture. The isotopologue fractionation factor for $^{13}CH_3D/^{12}CH_4$ is closely approximated by the product of those for $^{13}CH_4/^{12}CH_4$ and $^{12}CH_3D/^{12}CH_4$. Based on the isotopologue data, no significant degree of re-equilibration of C–H bonds in methane was detected.

Models were developed for simple scenarios involving variable fluxes of methane removed due to advection and oxidation. In open systems operating at steady state, $\Delta^{13}CH_3D$ values depend on the ratio of methane removed via

559 different processes, as well as the isotoplogue fractionation factors associated with those processes, whereas in
560 closed systems, $\Delta^{13}CH_3D$ values depend also on the fraction of methane remaining. Qualitative comparisons of
561 model predictions with available environmental $\Delta^{13}CH_3D$ data indicate that aerobic methane oxidation has only
562 minor, if any, influence on microbial methane samples reported to date to carry nonequilibrium $\Delta^{13}CH_3D$ values.
563 In combination with recent experimental and theoretical work on clumped isotopologue fractionation associated
564 with other methane sinks, the results of this study provide necessary constraints for the development of $^{13}CH_3D$ as
565 a tracer of the biogeochemical and atmospheric cycling of methane.

566 ## 6. ACKNOWLEDGMENTS

567 We thank J.H-C. Wei and W.J. Olszewski for technical assistance, and D.S. Gruen, R.E. Summons, J.W.
568 Pohlman, J.S. Seewald, and A.R. Whitehill for discussions. D.L. Valentine and two anonymous referees are
569 thanked for helpful and constructive reviews. Grants from the National Science Foundation (NSF EAR-1250394
570 to S.O. and EAR-1451767 to P.V.W.), and the Deep Carbon Observatory (to S.O.) supported this study. S.O.
571 thanks the Kerr-McGee Professorship at MIT. This research was conducted with Government support under and
572 awarded by U.S. Department of Defense, Office of Naval Research, National Defense Science and Engineering
573 Graduate (NDSEG) Fellowship (to D.T.W.), 32 CFR 168a.

574 ## 7. SUPPLEMENTARY DATA

575 Supplementary data associated with this manuscript can be found in the attached document.

576

577

578

579 **References**

580

581 Alperin M., Reeburgh W. and Whiticar M. (1988) Carbon and hydrogen isotope fractionation resulting from
582 anaerobic methane oxidation. *Global Biogeochemical Cycles* **2**, 279–288.

583 Bevington P. and Robinson D. K. (2002) *Data Reduction and Error Analysis for the Physical Sciences*. 3rd ed.,
584 McGraw-Hill Education.

585 Bigeleisen J. (1949) The relative reaction velocities of isotopic molecules. *The journal of chemical physics* **17**,
586 675.

587 Boetius A. and Wenzhöfer F. (2013) Seafloor oxygen consumption fuelled by methane from cold seeps. *Nature*
588 *Geoscience* **6**, 725–734.

589 Bousquet P., Ciais P., Miller J., Dlugokencky E., Hauglustaine D., Prigent C., Werf G. Van der, Peylin P., Brunke
590 E.-G., Carouge C. and others (2006) Contribution of anthropogenic and natural sources to atmospheric
591 methane variability. *Nature* **443**, 439–443.

592 Bowen G. J., Ehleringer J. R., Chesson L. A., Stange E. and Cerling T. E. (2007) Stable isotope ratios of tap water
593 in the contiguous United States. *Water Resources Research* **43**.

594 Bowman J. P. (2014) The family Methylococcaceae. In *The Prokaryotes* Springer. pp. 411–440.

595 Chanton J., Chasar L., Glaser P. and Siegel D. (2005) Carbon and hydrogen isotopic effects in microbial methane
596 from terrestrial environments. In *Stable Isotopes and Biosphere-Atmosphere Interactions, Physiological*
597 *Ecology Series* (eds. L. B. Flanagan, J. R. Ehleringer, and D. E. Pataki). Elsevier Academic Press London. pp.
598 85–105.

599 Cicerone R. J. and Oremland R. S. (1988) Biogeochemical aspects of atmospheric methane. *Global*
600 *Biogeochemical Cycles* **2**, 299–327.

601 Coleman D. D., Risatti J. B. and Schoell M. (1981) Fractionation of carbon and hydrogen isotopes by methane-
602 oxidizing bacteria. *Geochimica et Cosmochimica Acta* **45**, 1033–1037.

603 Coplen T. B. (2011) Guidelines and recommended terms for expression of stable-isotope-ratio and gas-ratio
604 measurement results. *Rapid Commun. Mass Spectrom.* **25**, 2538–2560.

605 Dlugokencky E. J., Nisbet E. G., Fisher R. and Lowry D. (2011) Global atmospheric methane: budget, changes
606 and dangers. *Philosophical Transactions of the Royal Society A: Mathematical, Physical and Engineering*
607 *Sciences* **369**, 2058–2072.

608 Douglas P., Stolper D., Smith D., Anthony K. W., Paull C., Dallimore S., Wik M., Crill P., Winterdahl M., Eiler
609 J. and others (2016) Diverse origins of Arctic and Subarctic methane point source emissions identified with
610 multiply-substituted isotopologues. *Geochimica et Cosmochimica Acta*.

611 Eiler J. M. (2007) Clumped-isotope“ geochemistry—The study of naturally-occurring, multiply-substituted
612 isotopologues. *Earth and Planetary Science Letters* **262**, 309–327.

613 Eiler J. M. and Schauble E. (2004) 18O 13C 16O in Earth’s atmosphere. *Geochimica et Cosmochimica Acta* **68**,
614 4767–4777.

Elsner M., Zwank L., Hunkeler D. and Schwarzenbach R. P. (2005) A new concept linking observable stable isotope fractionation to transformation pathways of organic pollutants. *Environmental science & technology* **39**, 6896–6916.

Ettwig K. F., Butler M. K., Le Paslier D., Pelletier E., Mangenot S., Kuypers M. M., Schreiber F., Dutilh B. E., Zedelius J., Beer D. de and others (2010) Nitrite-driven anaerobic methane oxidation by oxygenic bacteria. *Nature* **464**, 543–548.

Farquhar G. D., O'leary M. and Berry J. (1982) On the relationship between carbon isotope discrimination and the intercellular carbon dioxide concentration in leaves. *Australian Journal of Plant Physiology* **9**, 121–137.

Feilberg K. L., Griffith D. W., Johnson M. S. and Nielsen C. J. (2005) The 13C and D kinetic isotope effects in the reaction of CH4 with Cl. *International journal of chemical kinetics* **37**, 110–118.

Feisthauer S., Vogt C., Modrzynski J., Szlenkier M., Krüger M., Siegert M. and Richnow H.-H. (2011) Different types of methane monooxygenases produce similar carbon and hydrogen isotope fractionation patterns during methane oxidation. *Geochimica et Cosmochimica Acta* **75**, 1173–1184.

Green J. and Dalton H. (1989) Substrate specificity of soluble methane monooxygenase. Mechanistic implications. *Journal of Biological Chemistry* **264**, 17698–17703.

Hanson R. S. and Hanson T. E. (1996) Methanotrophic bacteria. *Microbiological Reviews* **60**, 439–471.

Harrison A. and Thode H. (1958) Mechanism of the bacterial reduction of sulphate from isotope fractionation studies. *Trans. Faraday Soc.* **54**, 84–92.

Hayes J. M. (2001) Fractionation of carbon and hydrogen isotopes in biosynthetic processes. *Reviews in mineralogy and geochemistry* **43**, 225–277.

Holler T., Wegener G., Knittel K., Boetius A., Brunner B., Kuypers M. M. and Widdel F. (2009) Substantial 13C/12C and D/H fractionation during anaerobic oxidation of methane by marine consortia enriched in vitro. *Environmental microbiology reports* **1**, 370–376.

Holler T., Wegener G., Niemann H., Deusner C., Ferdelman T. G., Boetius A., Brunner B. and Widdel F. (2011) Carbon and sulfur back flux during anaerobic microbial oxidation of methane and coupled sulfate reduction. *Proc. Natl. Acad. Sci. U. S. A.* **108**, E1484–E1490.

Horibe Y. and Craig H. (1995) D/H fractionation in the system methane-hydrogen-water. *Geochimica et cosmochimica acta* **59**, 5209–5217.

Hornibrook E. R., Longstaffe F. J. and Fyfe W. S. (1997) Spatial distribution of microbial methane production pathways in temperate zone wetland soils: stable carbon and hydrogen isotope evidence. *Geochimica et Cosmochimica Acta* **61**, 745–753.

Inagaki F., Hinrichs K.-U., Kubo Y., Bowles M., Heuer V., Hong W.-L., Hoshino T., Ijiri A., Imachi H., Ito M. and others (2015) Exploring deep microbial life in coal-bearing sediment down to 2.5 km below the ocean floor. *Science* **349**, 420–424.

IPCC (2013) *Climate change 2013: the physical science basis. Intergovernmental panel on climate change, working group I contribution to the IPCC fifth assessment report (AR5)*. eds. T. F. Stocker, D. Qin, G.

Plattner, M. Tignor, S. Allen, J. Boschung, A. Nauels, Y. Xia, V. Bex, and P. Midgley, New York: Cambridge University Press.

Joelsson L., Forecast R., Schmidt J., Meusinger C., Nilsson E., Ono S. and Johnson M. (2014) Relative rate study of the kinetic isotope effect in the 13 CH 3 D+ Cl reaction. *Chemical Physics Letters* **605**, 152–157.

Joelsson L., Schmidt J. A., Nilsson E., Blunier T., Griffith D., Ono S. and Johnson M. S. (2015) Development of a new methane tracer: kinetic isotope effect of 13 CH 3 D+ OH from 278 to 313 K. *Atmospheric Chemistry and Physics Discussions* **15**, 27853–27875.

Kai F. M., Tyler S. C., Randerson J. T. and Blake D. R. (2011) Reduced methane growth rate explained by decreased Northern Hemisphere microbial sources. *Nature* **476**, 194–197.

Kinnaman F. S., Valentine D. L. and Tyler S. C. (2007) Carbon and hydrogen isotope fractionation associated with the aerobic microbial oxidation of methane, ethane, propane and butane. *Geochimica et Cosmochimica Acta* **71**, 271–283.

Kirschke S., Bousquet P., Ciais P., Saunois M., Canadell J. G., Dlugokencky E. J., Bergamaschi P., Bergmann D., Blake D. R., Bruhwiler L. and others (2013) Three decades of global methane sources and sinks. *Nature Geoscience* **6**, 813–823.

Ku H. (1969) Notes on the use of propagation of error formulas. *J. Res. Nat. Bur. Stand. C* **70C**, 263–273.

Lau M. C., Stackhouse B., Layton A., Chauhan A., Vishnivetskaya T., Chourey K., Ronholm J., Mykytczuk N., Bennett P., Lamarche-Gagnon G., Burton N., Pollard W., Omelon C., Medvigy D., Hettich R., Pfiffner S., Whyte L. and Onstott T. (2015) An active atmospheric methane sink in high Arctic mineral cryosols. *The ISME journal* **9**, 1880–1891.

Mariotti A., Germon J., Hubert P., Kaiser P., Letolle R., Tardieux A. and Tardieux P. (1981) Experimental determination of nitrogen kinetic isotope fractionation: some principles; illustration for the denitrification and nitrification processes. *Plant and soil* **62**, 413–430.

Morrill P. L., Kuenen J. G., Johnson O. J., Suzuki S., Rietze A., Sessions A. L., Fogel M. L. and Nealson K. H. (2013) Geochemistry and geobiology of a present-day serpentinization site in California: The Cedars. *Geochimica et Cosmochimica Acta* **109**, 222–240.

Nesheim J. C. and Lipscomb J. D. (1996) Large kinetic isotope effects in methane oxidation catalyzed by methane monooxygenase: evidence for CH bond cleavage in a reaction cycle intermediate. *Biochemistry* **35**, 10240–10247.

Nihous G. C. (2008) A quantitative interpretation of recent experimental results on stable carbon isotope fractionation by aerobic CH 4-oxidizing bacteria. *Geochimica et Cosmochimica Acta* **72**, 4469–4475.

Nihous G. C. (2010) Notes on the temperature dependence of carbon isotope fractionation by aerobic CH4-oxidising bacteria. *Isotopes in Environmental and Health Studies* **46**, 133–140.

Ono S., Wang D. T., Gruen D. S., Sherwood Lollar B., Zahniser M., McManus B. J. and Nelson D. D. (2014) Measurement of a Doubly-Substituted Methane Isotopologue, 13CH3D, by Tunable Infrared Laser Direct Absorption Spectroscopy. *Analytical Chemistry* **86**, 6487–6494.

687 Oremland R. S. and Culbertson C. W. (1992) Importance of methane-oxidizing bacteria in the methane budget as
688 revealed by the use of a specific inhibitor. *Nature* **356**, 421–423.

689 Peterson E. J. R. (2005) Carbon and electron flow via methanogenesis, SO_4^2- , NO_3^- and Fe^3+ reduction in
690 the anoxic hypolimnia of upper Mystic Lake. Thesis, Massachusetts Institute of Technology.

691 Powelson D., Chanton J. and Abichou T. (2007) Methane oxidation in biofilters measured by mass-balance and
692 stable isotope methods. *Environmental Science & Technology* **41**, 620–625.

693 Pudzianowski A. T. and Loew G. H. (1983) Hydrogen abstractions from methyl groups by atomic oxygen.
694 Kinetic isotope effects calculated from MNDO/UHF results and an assessment of their applicability to
695 monooxygenase-dependent hydroxylations. *The Journal of Physical Chemistry* **87**, 1081–1085.

696 Rasigraf O., Vogt C., Richnow H.-H., Jetten M. S. and Ettwig K. F. (2012) Carbon and hydrogen isotope
697 fractionation during nitrite-dependent anaerobic methane oxidation by Methylomirabilis oxyfera. *Geochimica*
698 *et Cosmochimica Acta* **89**, 256–264.

699 Rataj M., Kauth J. and Donnelly M. (1991) Oxidation of deuterated compounds by high specific activity methane
700 monooxygenase from Methylosinus trichosporium. Mechanistic implications. *Journal of Biological*
701 *Chemistry* **266**, 18684–18690.

702 Reeburgh W. S. (1976) Methane consumption in Cariaco Trench waters and sediments. *Earth and Planetary*
703 *Science Letters* **28**, 337–344.

704 Reeburgh W. S. (2007) Oceanic methane biogeochemistry. *Chemical Reviews* **107**, 486–513.

705 Rees C. (1973) A steady-state model for sulphur isotope fractionation in bacterial reduction processes. *Geochim.*
706 *Cosmochim. Acta* **37**, 1141–1162.

707 Rigby M., Manning A. and Prinn R. (2012) The value of high-frequency, high-precision methane isotopologue
708 measurements for source and sink estimation. *Journal of Geophysical Research: Atmospheres (1984–2012)*
709 **117**.

710 Saueressig G., Bergamaschi P., Crowley J., Fischer H. and Harris G. (1995) Carbon kinetic isotope effect in the
711 reaction of CH4 with Cl atoms. *Geophysical Research Letters* **22**, 1225–1228.

712 Saueressig G., Bergamaschi P., Crowley J., Fischer H. and Harris G. (1996) D/H kinetic isotope effect in the
713 reaction CH4+ Cl. *Geophysical Research Letters* **23**, 3619–3622.

714 Saueressig G., Crowley J. N., Bergamaschi P., Brühl C., Brenninkmeijer C. A. and Fischer H. (2001) Carbon 13
715 and D kinetic isotope effects in the reactions of CH4 with O (1 D) and OH: New laboratory measurements
716 and their implications for the isotopic composition of stratospheric methane. *Journal of Geophysical*
717 *Research: Atmospheres (1984–2012)* **106**, 23127–23138.

718 Scheller S., Goenrich M., Boecher R., Thauer R. K. and Jaun B. (2010) The key nickel enzyme of methanogenesis
719 catalyses the anaerobic oxidation of methane. *Nature* **465**, 606–608.

720 Sessions A. L. and Hayes J. M. (2005) Calculation of hydrogen isotopic fractionations in biogeochemical
721 systems. *Geochimica et Cosmochimica Acta* **69**, 593–597.

722 Sirajuddin S. and Rosenzweig A. C. (2015) Enzymatic oxidation of methane. *Biochemistry* **54**, 2283–2294.

Stolper D. A., Lawson M., Davis C. L., Ferreira A. A., Santos Neto E. V., Ellis G. S., Lewan M. D., Martini A. M., Tang Y., Schoell M., Sessions A. L. and Eiler J. M. (2014a) Formation temperatures of thermogenic and biogenic methane. *Science* **344**, 1500–1503.

Stolper D. A., Sessions A. L., Ferreira A. A., Neto E. V. S., Schimmelmann A., Shusta S. S., Valentine D. L. and Eiler J. M. (2014b) Combined 13C-D and D-D clumping in methane: methods and preliminary results. *Geochimica et Cosmochimica Acta* **126**, 169–191.

Stolper D., Martini A., Clog M., Douglas P., Shusta S., Valentine D., Sessions A. and Eiler J. (2015) Distinguishing and understanding thermogenic and biogenic sources of methane using multiply substituted isotopologues. *Geochimica et Cosmochimica Acta* **161**, 219–247.

Takai K., Nakamura K., Toki T., Tsunogai U., Miyazaki M., Miyazaki J., Hirayama H., Nakagawa S., Nunoura T. and Horikoshi K. (2008) Cell proliferation at 122 C and isotopically heavy CH4 production by a hyperthermophilic methanogen under high-pressure cultivation. *Proceedings of the National Academy of Sciences* **105**, 10949–10954.

Templeton A. S., Chu K.-H., Alvarez-Cohen L. and Conrad M. E. (2006) Variable carbon isotope fractionation expressed by aerobic CH< sub> 4</sub>-oxidizing bacteria. *Geochimica et Cosmochimica Acta* **70**, 1739–1752.

Tyler S. C., Ajie H. O., Rice A. L., Cicerone R. J. and Tuazon E. C. (2000) Experimentally determined kinetic isotope effects in the reaction of CH4 with Cl: Implications for atmospheric CH4. *Geophysical Research Letters* **27**, 1715–1718.

Valentine D. L. (2011) Emerging topics in marine methane biogeochemistry. *Annual Review of Marine Science* **3**, 147–171.

Valentine D. L., Chidthaisong A., Rice A., Reeburgh W. S. and Tyler S. C. (2004) Carbon and hydrogen isotope fractionation by moderately thermophilic methanogens. *Geochimica et Cosmochimica Acta* **68**, 1571–1590.

Vavilin V. A., Rytov S. V., Shim N. and Vogt C. (2015) Non-linear dynamics of stable carbon and hydrogen isotope signatures based on a biological kinetic model of aerobic enzymatic methane oxidation. *Isotopes in environmental and health studies*, 1–18.

Wahlen M. (1993) The global methane cycle. *Annual Review of Earth and Planetary Sciences* **21**, 407–426.

Wang D. T., Gruen D. S., Lollar B. S., Hinrichs K.-U., Stewart L. C., Holden J. F., Hristov A. N., Pohlman J. W., Morrill P. L., Könneke M., Delwiche K. B., Reeves E. P., Sutcliffe C. N., Ritter D. J., Seewald J. S., McIntosh J. C., Hemond H. F., Kubo M. D., Cardace D., Hoehler T. M. and Ono S. (2015) Nonequilibrium clumped isotope signals in microbial methane. *Science* **348**, 428–431.

Wang Z., Schauble E. A. and Eiler J. M. (2004) Equilibrium thermodynamics of multiply substituted isotopologues of molecular gases. *Geochimica et Cosmochimica Acta* **68**, 4779–4797.

Ward N., Larsen Ø., Sakwa J., Bruseth L., Khouri H., Durkin A. S., Dimitrov G., Jiang L., Scanlan D., Kang K. H., Lewis M., Nelson K. E., Methé B., Wu M., Heidelberg J. F., Paulsen I. T., Fouts D., Ravel J., Tettelin H., Ren Q., Read T., DeBoy R. T., Seshadri R., Salzberg S. L., Jensen H. B., Birkeland N. K., Nelson W. C., Dodson R. J., Grindhaug S. H., Holt I., Eidhammer I., Jonasen I., Vanaken S., Utterback T., Feldblyum T. V., Fraser C. M., Lillehaug J. R. and Eisen J. A. (2004) Genomic Insights into Methanotrophy: The Complete Genome Sequence of Methylococcus capsulatus (Bath). *PLoS Biol* **2**, e303.

Welander P. V. and Summons R. E. (2012) Discovery, taxonomic distribution, and phenotypic characterization of a gene required for 3-methylhopanoid production. *Proceedings of the National Academy of Sciences* **109**, 12905–12910.

Whitehill A. R., Joelsson L. M. T., Schmidt J. A., Wang D. T., Johnson M. S. and Ono S. Clumped isotope effects during OH and Cl oxidation of methane. *Geochimica et Cosmochimica Acta* **submitted**.

Whiticar M. J. (1999) Carbon and hydrogen isotope systematics of bacterial formation and oxidation of methane. *Chemical Geology* **161**, 291–314.

Whiticar M. and Schaefer H. (2007) Constraining past global tropospheric methane budgets with carbon and hydrogen isotope ratios in ice. *Philosophical Transactions of the Royal Society A: Mathematical, Physical and Engineering Sciences* **365**, 1793–1828.

Whittenbury R., Phillips K. and Wilkinson J. (1970) Enrichment, isolation and some properties of methane-utilizing bacteria. *Journal of General Microbiology* **61**, 205–218.

Wilkins P. C., Dalton H., Samuel C. J. and Green J. (1994) Further Evidence for Multiple Pathways in Soluble Methane-Monooxygenase-Catalysed Oxidations from the Measurement of Deuterium Kinetic Isotope Effects. *European Journal of Biochemistry* **226**, 555–560.

Yeung L. Y. (2016) Combinatorial effects on clumped isotopes and their significance in biogeochemistry. *Geochimica et Cosmochimica Acta* **172**, 22–38.

Yeung L. Y., Young E. D. and Schauble E. A. (2012) Measurements of 18O18O and 17O18O in the atmosphere and the role of isotope-exchange reactions. *Journal of Geophysical Research: Atmospheres (1984–2012)* **117**.

Yoshinaga M. Y., Holler T., Goldhammer T., Wegener G., Pohlman J. W., Brunner B., Kuypers M. M., Hinrichs K.-U. and Elvert M. (2014) Carbon isotope equilibration during sulphate-limited anaerobic oxidation of methane. *Nature Geoscience* **7**, 190–194.

Yoshizawa K. and Yumura T. (2003) A Non-Radical Mechanism for Methane Hydroxylation at the Diiron Active Site of Soluble Methane Monooxygenase. *Chemistry-A European Journal* **9**, 2347–2358.

Young E. D., Rumble D., Freedman P. and Mills M. (2016) A large-radius high-mass-resolution multiple-collector isotope ratio mass spectrometer for analysis of rare isotopologues of O 2, N 2, CH 4 and other gases. *International Journal of Mass Spectrometry* **401**, 1–10.

8. FIGURES

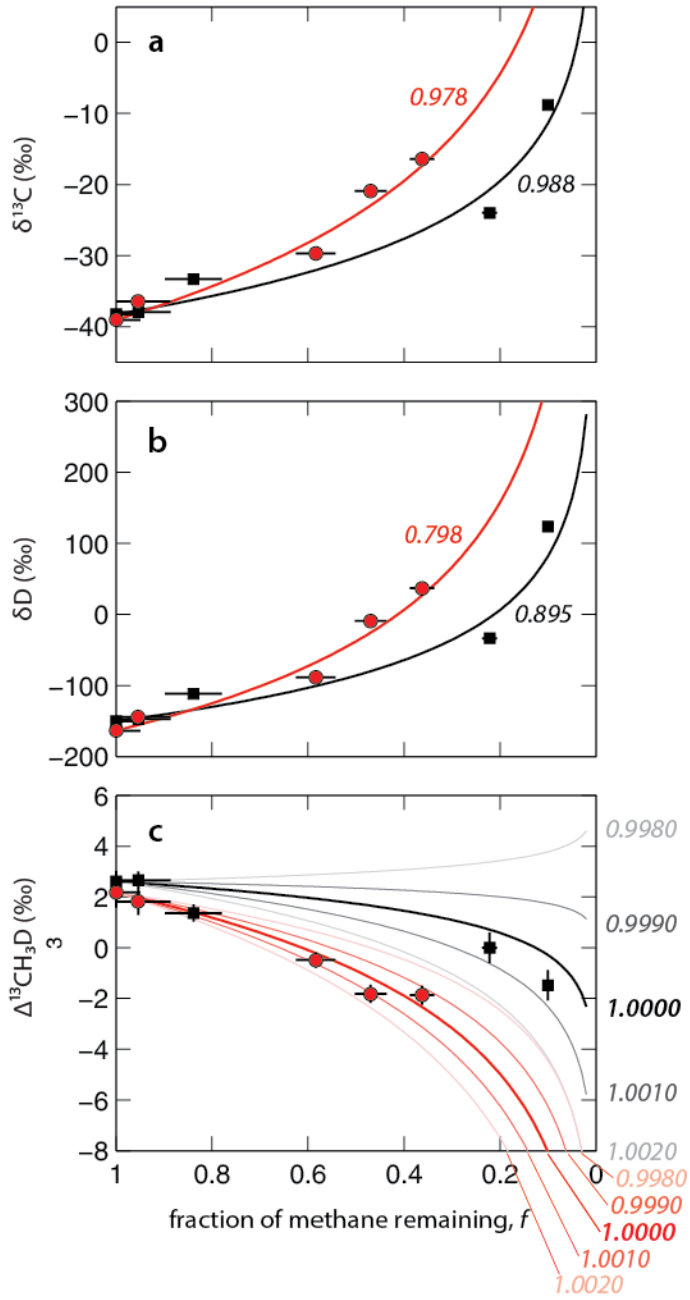

Fig. 1. Measured and modeled changes in (a) $\delta^{13}C$, (b) δD, and (c) $\Delta^{13}CH_3D$ of residual methane as a function of *f*, the fraction of initial methane remaining. Data points from the 30 and 37 °C experiments (Table 1) are shown with black and red symbols, respectively. Horizontal error bars represent propagated ±1σ uncertainties from GC measurements, and vertical error bars represent 95% confidence intervals from isotopologue ratio analyses. Solid lines represent the modeled values (from Eqns. 13, 16, and 20) based on the calculated weighted-average carbon- and hydrogen-isotope fractionation factors for each set of experiments as listed in Table 1. Labels in *italics*

represent $^{13}\alpha$, $^{D}\alpha$, & γ, respectively, in panels (a), (b), & (c). Panel (c) shows model results calculated assuming different values of γ varying between 0.9980 and 1.0020.

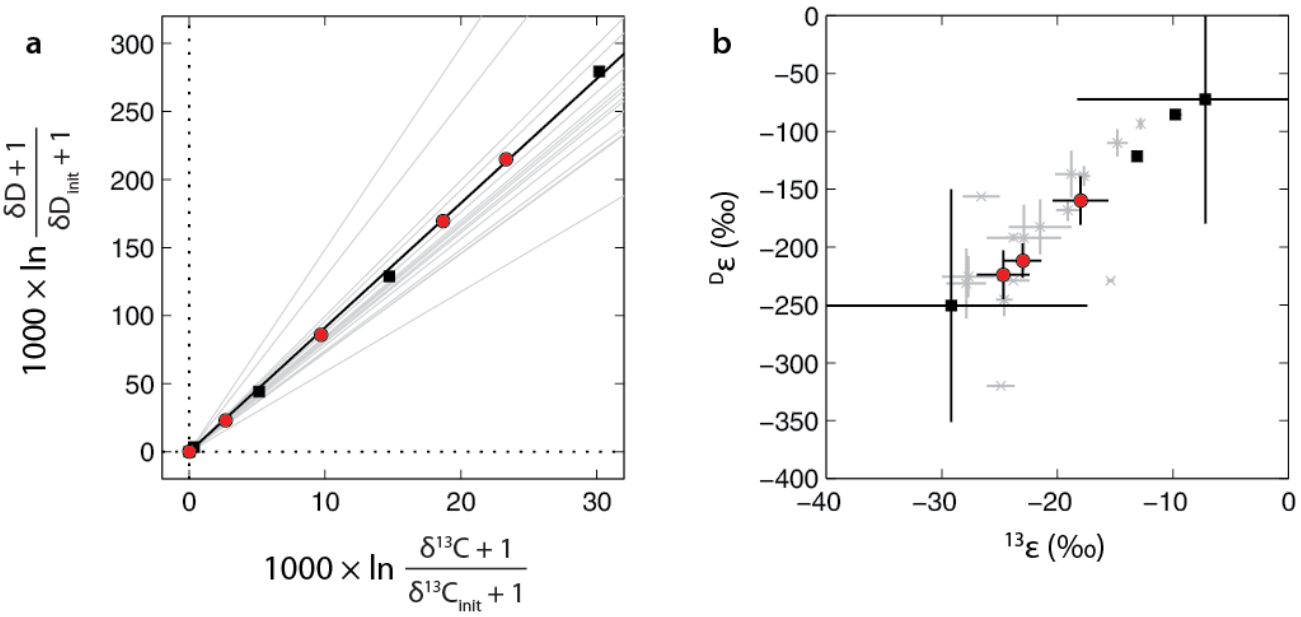

Fig. 2. Relationship between fractionation of carbon and hydrogen isotopes. (a) Data from the 30 and 37 °C experiments (Table 1) are shown with black and red symbols, respectively. Black line ($y = 9.14\ x$) represents the best-fit regression through the data. From Eqn. 17, the slope of this line is $({}^{D}\alpha - 1)/({}^{13}\alpha - 1)$, or ${}^{D}\varepsilon/{}^{13}\varepsilon$. Near the origin, the x- and y-axes are approximately equal to $\delta^{13}C - \delta^{13}C_{init}$ and $\delta D - \delta D_{init}$, respectively; this approximation becomes less accurate with increasing distance from the origin, particularly for hydrogen (Sessions and Hayes, 2005). Gray lines represent previously-reported correlations between fractionation of carbon and hydrogen isotopes by aerobic methanotrophs determined from experiments with pure cultures (Feisthauer et al., 2011) and enrichment cultures (Coleman et al., 1981; Kinnaman et al., 2007; Powelson et al., 2007). (b) Fractionation factors (ε, defined as α − 1) calculated for individual bottle incubations from this study (Table 1) plotted against fractionation factors reported in the cited studies (gray). One point from the 37 °C experiment (41 h) was not plotted because of large uncertainties arising from a minimal extent of reaction.

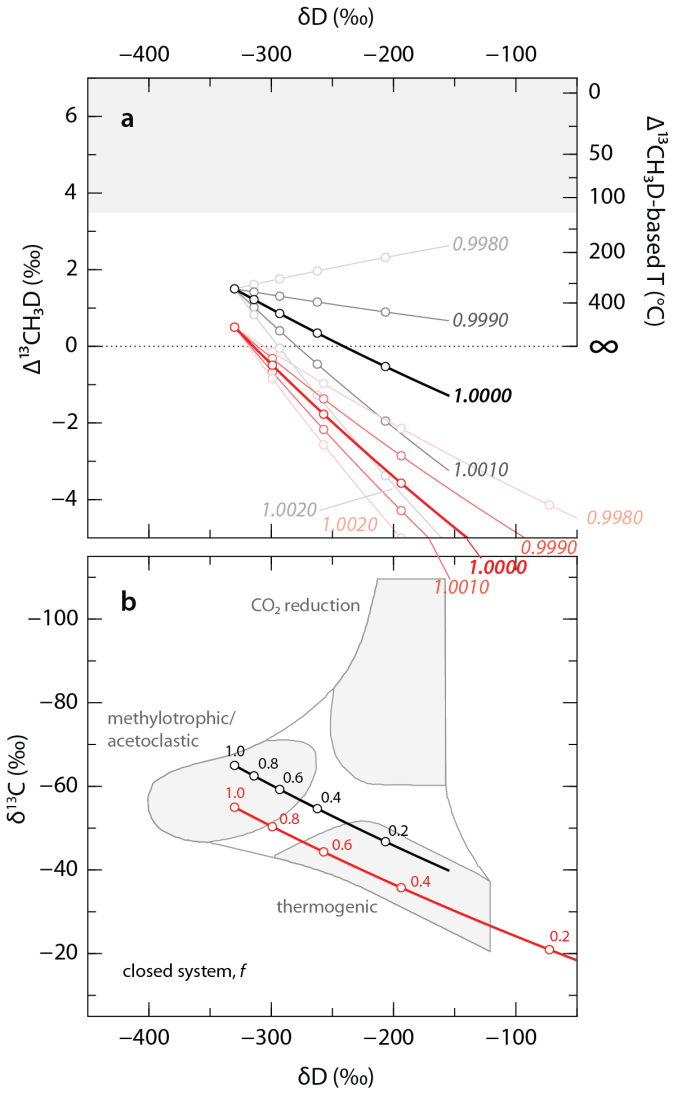

Fig. 3. Modeled changes in (a) $\Delta^{13}CH_3D$ vs. δD and (b) $\delta^{13}C$ vs. δD of residual methane during aerobic methane oxidation under closed system conditions. Solid lines represent model predictions (from Eqns. 13, 16, and 20) based on the calculated weighted-average carbon- and hydrogen-isotope fractionation factors for each set of experiments (black, 30 °C; red, 37 °C) as listed in Table 1 and shown in Fig. 1. Labels in *italics* in panel (a) represent γ values. Circles are marked at intervals of 0.2 in *f*, the fraction of initial methane remaining, and labeled in panel (b). For visual clarity, the models were initialized at slightly different $\delta^{13}C$ and $\Delta^{13}CH_3D$ values. The initial isotope values were chosen for illustrative purposes only and do not represent any particular natural sample; however, the chosen values are typical of modern microbial methane generated in wetland and lake sediments. Following Wang et al. (2015), the gray field in panel (a) represents the temperature range within which microbial life has been shown to occur (Takai et al., 2008), and the gray fields in panel (b) represent empirical methane source fields suggested by Whiticar (1999).

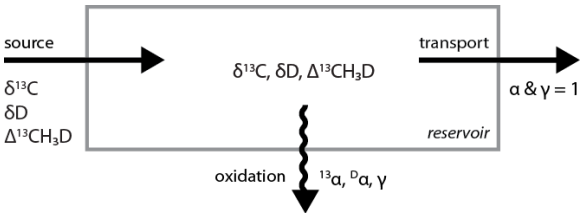

829

830 Fig. 4. Representation of a model open system in which methane is transported in and out via advection, and in
831 which aerobic methane oxidation is also occurring. The fractional contribution of oxidation to the total sinks is
832 φ_{ox}. See Fig. 5 and discussion in Sec. 4.2.1.

833

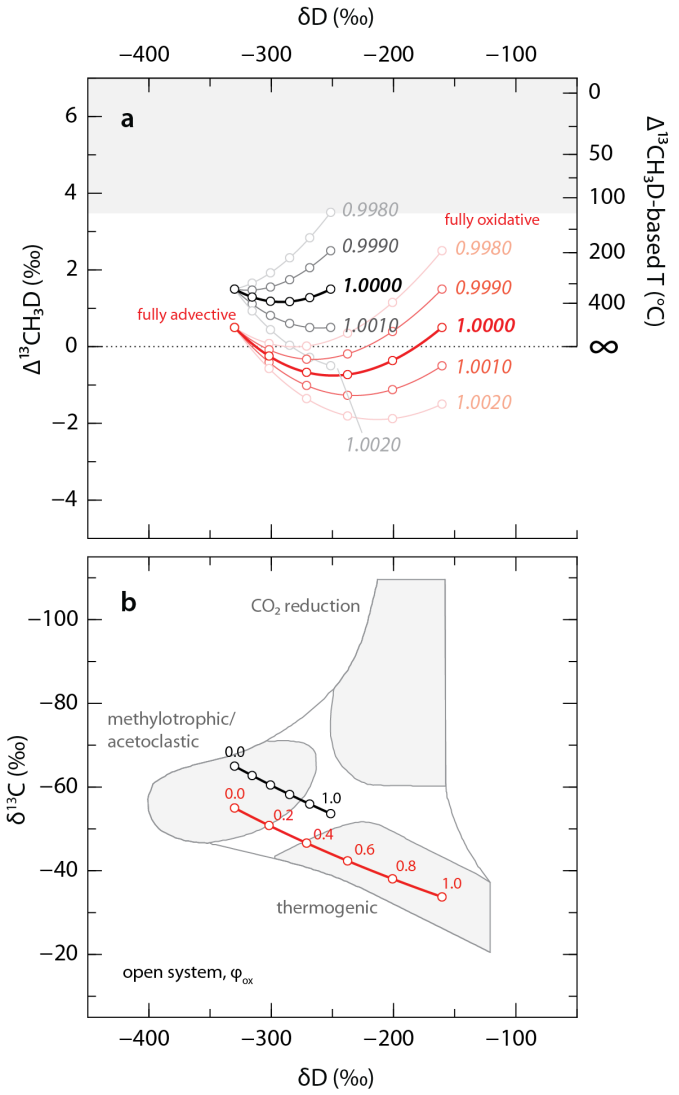

Fig. 5. Modeled steady-state values of (a) $\Delta^{13}CH_3D$ vs. δD and (b) $\delta^{13}C$ vs. δD of methane in an open system (Fig. 4) consisting of a single source and two sinks (aerobic methane oxidation and advection). Advection is assumed to be non-fractionating. Lines were modeled using Eqns. 22 and 23, and the same fractionation factors for aerobic methane oxidation as for those shown with the same line style in Fig. 2. Labels in *italics* in panel (a) represent γ values associated with aerobic methane oxidation. Circles are marked at intervals of 0.2 in φ_{ox}, the fraction of methane removed via oxidation, ranging from fully advective ($\varphi_{ox} = 0$) to fully oxidative ($\varphi_{ox} = 1$), and labeled in panel (b). When $\varphi_{ox} = 0$, the isotopic composition of methane in the reservoir is identical to that of the source. For visual clarity, the calculations were performed for slightly different $\delta^{13}C$ and $\Delta^{13}CH_3D$ values of input methane. For description of shaded fields, see the caption for Fig. 3.

9. TABLES

Table 1

Experimental results and calculated fractionation factors for batch cultures of *Methylococcus capsulatus* Bath. Uncertainties (±1σ) listed for *f*, $^{13}\alpha$, $^{D}\alpha$, and γ are propagated from those associated with individual measurements according to standard formulas (Ku, 1969).

	time (h)	*f*	CO_2 (cm^3)[a]	$\delta^{13}C$ (‰)[c]	δD (‰)[c]	$\Delta^{13}CH_3D$ (‰)[c]	$^{13}\alpha$	$^{D}\alpha$	γ
30 °C	0	1.00 ± 0.05[b]	<0.2	−38.27	−150.12	2.61 ± 0.43			
	12	0.95 ± 0.07	0.6	−37.94	−147.20	2.66 ± 0.34	0.993 ± 0.011	0.928 ± 0.107	0.9983 ± 0.0130
	36	0.84 ± 0.06	1.9	−33.31	−111.79	1.36 ± 0.34	0.971 ± 0.012	0.749 ± 0.101	0.9997 ± 0.0060
	–[d]	0.22 ± 0.02	10.3	−24.00	−33.36	−0.01 ± 0.60	0.990 ± 0.0005	0.915 ± 0.004	1.0010 ± 0.0005
	60	0.10 ± 0.01	9.8	−8.81	123.90	−1.48 ± 0.60	0.987 ± 0.0004	0.878 ± 0.004	1.0002 ± 0.0004
						weighted average[e]	0.988 ± 0.0003	0.895 ± 0.003	1.0005 ± 0.0003
37 °C	0	1.00 ± 0.05[b]	n.d.	−39.06	−163.57	2.17 ± 0.59			
	41	0.95 ± 0.07	n.d.	−36.45	−144.23	1.82 ± 0.53	0.943 ± 0.086	0.516 ± 0.726	0.9585 ± 0.2130
	44	0.58 ± 0.04	2.5	−29.68	−88.51	−0.48 ± 0.30	0.982 ± 0.002	0.840 ± 0.021	1.0025 ± 0.0015
	48	0.47 ± 0.03	4.8	−20.95	−9.20	−1.82 ± 0.36	0.975 ± 0.002	0.776 ± 0.021	0.9997 ± 0.0014
	51	0.36 ± 0.03	6.3	−16.39	36.83	−1.87 ± 0.38	0.977 ± 0.002	0.788 ± 0.015	0.9989 ± 0.0011
						weighted average[e]	0.978 ± 0.001	0.798 ± 0.010	1.0000 ± 0.0007

n.d., not determined

[a] Total inorganic carbon in the bottle (including gaseous CO_2 and dissolved inorganic carbon), reported as cm^3-equivalent of CO_2 at standard ambient temperature and pressure (SATP; 25 °C, 1 bar), was estimated from headspace CO_2 concentration (determined via GC), the Henry's law constant for CO_2 at room temperature, and the volume of headspace and of HCl-spiked medium. Uncertainty is estimated at ±10%. Quantitative conversion of initial CH_4 (see Sec. 2.1) into CO_2 (i.e., 100% oxidation with no incorporation of CH_4-derived carbon into biomass) would yield 20 cm^3 SATP of CO_2.

[b] An uncertainty of ±5% was assigned to the initial value of *f* to account for variability in starting amounts of methane between bottles (see Sec. 2.1). This uncertainty is propagated throughout the calculations for later timepoints.

[c] Values for $\delta^{13}C$, δD, and $\Delta^{13}CH_3D$ are reported relative to PDB, SMOW, and the stochastic distribution, respectively. Uncertainties for $\delta^{13}C$, δD (both ca. 0.1‰), and $\Delta^{13}CH_3D$ (listed) are 95% confidence intervals.

[d] Time not recorded.

[e] Weighted means of each set of $^{13}\alpha$, $^{D}\alpha$, and γ values, weighted by $1/\sigma^2$. Uncertainty (1σ) in weighted means was estimated following Bevington and Robinson (2002).

869 Table 2

870 Comparison of experimentally-determined ratios of carbon- and hydrogen-isotope fractionation factors ($^{D}\varepsilon/^{13}\varepsilon$) and $^{13}CH_3D$
871 fractionation factors (γ) for different methane sink processes. Uncertainties quoted are ±2σ or 95% confidence interval.

	$^{D}\varepsilon/^{13}\varepsilon$	γ
Aerobic methane oxidation		
Previous work[a]	5.9 to 14.9	
This study[b]	9.14 ± 0.14	1.0004 ± 0.0006
Anaerobic oxidation of methane (AOM)		
Holler et al. (2009)	6.4 to 8.5	
Nitrite-dependent anaerobic methane oxidation		
Rasigraf et al. (2012)	7.8 ± 0.8	
CH_4 + OH		
Saueressig et al. (2001)	58.5 ± 6.6	
Joelsson et al. (2014)		0.980 ± 0.038
Whitehill et al. (in revision)	41.3 ± 8.3	0.9997 ± 0.0012
CH_4 + Cl		
Tyler et al. (2000)	5.51	
Saueressig et al. (1995; 1996)	5.50	
Feilberg et al. (2005)	5.65	
Joelsson et al. (2015)		0.978 ± 0.051
Whitehill et al. (in revision)	5.56	0.9965 ± 0.0007

872

873 [a] See caption of Fig. 2a for references. Also see Rasigraf et al. (2012) for a compilation of $^{13}\varepsilon$ and $^{D}\varepsilon$ values determined for
874 biological methane oxidation in cultures and in the environment.
875 [b] Derived from linear regression ($^{D}\varepsilon/^{13}\varepsilon$, Fig. 2a) or weighted average (γ) of all timepoints in both experiments in Table 1.
876